Energy & Environmental Science

Cite this: *Energy Environ. Sci.*, 2012, **5**, 9653

www.rsc.org/ees

PAPER

Hydrogen-evolution characteristics of Ni–Mo-coated, radial junction, n$^+$p-silicon microwire array photocathodes†

Emily L. Warren,[a] James R. McKone,[a] Harry A. Atwater,[bc] Harry B. Gray[a] and Nathan S. Lewis*[ac]

Received 16th August 2012, Accepted 13th September 2012
DOI: 10.1039/c2ee23192a

The photocathodic H_2-evolution performance of Ni–Mo-coated radial n$^+$p junction Si microwire (Si MW) arrays has been evaluated on the basis of thermodynamic energy-conversion efficiency as well as solar cell figures of merit. The Ni–Mo-coated n$^+$p-Si MW electrodes yielded open-circuit photovoltages (V_{oc}) of 0.46 V, short-circuit photocurrent densities (J_{sc}) of 9.1 mA cm^{-2}, and thermodynamically based energy-conversion efficiencies (η) of 1.9% under simulated 1 Sun illumination. Under nominally the same conditions, the efficiency of the Ni–Mo-coated system was comparable to that of Pt-coated n$^+$p-Si MW array photocathodes ($V_{oc} = 0.44$ V, $J_{sc} = 13.2$ mA cm^{-2}, $\eta = 2.7\%$). This demonstrates that, at 1 Sun light intensity on high surface area microwire arrays, earth-abundant electrocatalysts can provide performance comparable to noble-metal catalysts for photoelectrochemical hydrogen evolution. The formation of an emitter layer on the microwires yielded significant improvements in the open-circuit voltage of the microwire-array-based photocathodes relative to Si MW arrays that did not have a buried n$^+$p junction. Analysis of the spectral response and light-intensity dependence of these devices allowed for optimization of the catalyst loading and photocurrent density. The microwire arrays were also removed from the substrate to create flexible, hydrogen-evolving membranes that have potential for use in a solar water-splitting device.

Introduction

The structuring of light absorbers, such as Si, into microwire- and/or nanowire-based morphologies orthogonalizes the directions of light absorption and carrier collection, and thus provides an opportunity to obtain high solar energy-conversion efficiencies with low purity semiconductor materials.[1] Accordingly, arrays of p-type Si microwires (MW) grown by the vapor–liquid–solid (VLS) process have shown >3% solar energy-conversion efficiencies as photocathodes in regenerative electrochemical cells.[2,3] Solid-state photovoltaic devices made from n$^+$p radial junction Si MW arrays have also yielded >7% energy-conversion efficiency under 100 mW cm^{-2} (1 Sun) of simulated Air Mass 1.5 global (AM 1.5G) illumination.[4,5] These same Si MW array structures, when coated with Pt as a catalyst for the hydrogen-evolution reaction (HER), have produced thermodynamically

[a]*Division of Chemistry and Chemical Engineering, California Institute of Technology, 1200 E. California Blvd, Pasadena, CA 91125, USA*
[b]*Thomas J. Watson Laboratories of Applied Physics, California Institute of Technology, 1200 E. California Blvd, Pasadena, CA 91125, USA*
[c]*Kavli Nanoscience Institute, California Institute of Technology, 1200 E. California Blvd, Pasadena, CA 91125, USA*

† Electronic supplementary information (ESI) available. See DOI: 10.1039/c2ee23192a

Broader context

An integrated artificial photosynthetic system, capable of directly converting solar energy to chemical fuel, remains a challenge for the development of low-cost, scalable storage of solar energy. A tandem photoelectrochemical cell that consists of an integrated oxygen-evolving photoanode and a hydrogen-evolving photocathode can allow for optimal utilization of the solar spectrum to achieve the >1.23 V required to drive the water-splitting reaction. Silicon is an attractive candidate for a tandem-system photocathode because Si is earth abundant, has an ideal bandgap (1.1 eV) for a dual-absorber system, and is stable under cathodic conditions in acidic aqueous systems. Si microwire arrays can be grown from inexpensive precursors and can be embedded in a polymer to produce flexible, crystalline Si solar cells with the potential to reach efficiencies comparable to those of wafer-based Si devices. We describe the coupling of earth-abundant hydrogen-evolution catalysts to Si microwire arrays, resulting in a photocathode for the production of hydrogen that does not rely on rare absorber or catalyst materials.

based photocathodic energy-conversion efficiencies of >5% under 1 Sun illumination, despite only absorbing ~50% of the incident photons with energies larger than the band-gap energy of Si.[6]

For photoelectrochemical applications, the high surface area of MW array structures facilitates a high catalyst loading onto a given projected area of the electrode. On a projected-area basis, this increased loading allows, in principle, non-precious-metal electrocatalysts to yield comparable performance to noble-metal catalysts, such as Pt, for multi-electron-transfer processes such as H_2 production from H_2O.[7,8] For H_2-evolution from aqueous solution at pH = 4.5, degenerately doped n^+-Si MW electrodes coated with Ni–Mo have shown comparable electrochemical performance to Pt-coated n^+-Si MW arrays.[7] However, p-Si MW array photocathodes coated with a Ni–Mo catalyst have been reported to exhibit photovoltages of only 150 mV.[7] Earth-abundant catalysts have been coupled, through a conductive overlayer, to drive the overall water splitting reaction using commercially available photovoltaic cells.[9,10] However, earth-abundant catalysts directly coupled to semiconductor absorbers have not yet exhibited the ability to simultaneously affect the HER at low overpotentials while also generating a significant portion of the photovoltage that is necessary to spontaneously drive the water-splitting reaction.[8,11,12]

In this work, Ni–Mo has been deposited onto n^+p-Si MW arrays, with the goal of creating efficient H_2-evolving photocathodes that consist only of earth-abundant materials. The effects of catalyst loading, morphology, and semiconductor device characteristics on the photocathode performance have been investigated for Ni–Mo-coated n^+p-junction Si MW arrays attached to a degenerately doped (photo-inactive) Si growth wafer; for Ni–Mo-coated n^+p planar Si junctions; for Ni–Mo-coated p-Si MW arrays; and for Pt-coated n^+p-Si MW arrays. We have also prepared freestanding polymer-supported membranes based on Ni–Mo-coated n^+p-Si MW microwire arrays, and have compared the performance of such systems to the behavior of the Si MW arrays that were physically connected to the crystalline Si growth substrate.

Experimental methods

A. Wire growth and n^+p junction formation

To produce substrates for the controlled growth of patterned Si MWs, degenerately doped p-type (111)-oriented Si wafers (with a resistivity, $\rho < 0.003$ Ω cm) were coated with 350–500 nm of thermally grown SiO_2 (Silicon Quest International or University Wafers) and were patterned using standard photolithographic methods. A photoresist layer (Shipley 1813, Microchem) was deposited on the oxide, with the photoresist exposed to produce a square array of 3 μm diameter, circular holes with a hole-to-hole pitch of 7 μm. The SiO_2 exposed through the holes in the photoresist layer was etched using buffered HF (Transene Inc.) to reveal the underlying Si substrate. 400–600 nm of Cu (EPSI 6N) was then thermally evaporated onto the substrate, and the excess metal and photoresist were removed with acetone. Si MWs were then grown by the vapor–liquid–solid (VLS) growth method, in which the samples (~1.5 × 2 cm) were annealed in a H_2 atmosphere at 1000 °C for 20–25 min, followed by exposure to flowing $SiCl_4$ (Strem, 6N) saturated in He or H_2. BCl_3 (0.25% in H_2, Matheson) and H_2 were also introduced into the reaction chamber, with a $SiCl_4/BCl_3/H_2$ ratio of 50 : 0.5–2 : 500. The length of the wires was controlled by the growth time (15–22 min) as well as by the position of the substrate in the reactor. After wire growth, the samples were cooled to ~600 °C under H_2, cooled to room temperature under He, and then removed from the reactor.

The Cu growth catalyst was removed from the Si wires by use of a 15 min RCA2 etch (5 : 1 : 1 H_2O : HCl : H_2O_2 at 70 °C), followed by a 20–30 s etch in 4 M KOH (aq.) (Aldrich, semiconductor grade), and then by a second RCA2 etch. To fabricate the radial n^+p junctions, a dry, 150 nm thick, thermal oxide was grown over the surface of the Si wires. A mixture of uncured polydimethylsiloxane (PDMS, Sylgard 184, Dow Corning) and an organic solvent (methylene chloride or toluene) was spin-coated onto the samples at ~1000 rpm, and the samples were cured on a hot plate. Before curing, almost all of the PDMS settled to the bottom 10–20 μm of the array, and any residual PDMS film was etched off using a plasma ash or a PDMS-etching solution. Buffered HF was then used to etch the oxide off of the tops of the wires. The PDMS was then removed from the samples by use of a mixture of tetrabutylammonium fluoride (TBAF) and 1-methyl-2-pyrrolidone (NMP) (3 : 1; v/v; NMP/75% TBAF in water).[13] Residual organics were removed by a 10 min Piranha clean (4 : 1 sulfuric acid : hydrogen peroxide), followed by a 15 min RCA1 (5 : 1 : 1 H_2O : NH_4OH : H_2O_2 at 70 °C) clean, followed by a RCA2 clean. Planar devices were subjected to the same RCA1/RCA2 cleaning process prior to formation of an emitter layer.

Samples were doped by heating the Si substrates between solid CeP_2O_{14} doping wafers (Saint-Gobain, PH-900 PDS). The samples were annealed for 10–15 min at 850 °C. On planar devices, this process produced a 100–150 nm thick n^+ emitter layer that had a sheet resistance of 95–120 Ω sq^{-1}. The Si MW arrays were immersed for 30 s in buffered HF, to remove from the Si surface the P_2O_5 glass that formed during doping.

The bases of the Si MW arrays were infilled with either alumina (Sasol Cerelix APA 0.5AF) or titania-based (Dupont Ti-Pure R-105) scattering particles, embedded in PDMS (30–50 μm). The PDMS protected the p-Si–n^+-Si interface from exposure to the electrolyte. PDMS was removed from the tips of the wires by a 60–180 s etch in an O_2 plasma (300 mW, 300 mTorr), followed by a 30 s dip in the PDMS etch solution, and then by a 60 s immersion in buffered HF. The doping densities of as-grown wires, and the diode behavior of n^+p radial junction wires, were measured by lithographically defined contacts to the ends of individual Si wires that had been scraped from the surface.[4]

B. Electrode fabrication

Samples were either cut directly into electrodes (with areas 0.02–0.10 cm^{-2}) or were peeled from the substrate before use. Ga/In eutectic was used to make back contact to the degenerately doped Si substrates that had Si MW arrays attached to the front surface of the sample. For planar Si samples, 100 nm of Al was evaporated on the back of the sample, and such samples were annealed under forming gas at 800 °C for 10 min, to create a p^+ back-surface field. Ag paint was used to mount the electrodes

onto coiled Cu wire. The mounted electrodes were sealed into a glass tube using insulating epoxy (Loctite 9460 and Hysol 1C).

Freestanding polymer-supported membranes were fabricated by use of a razor blade to mechanically remove the PDMS-embedded wire arrays from the growth substrate. Ohmic contact was made to the peeled membranes by electron-beam evaporation (TES, Inc.) of 200–300 nm of Au (Lesker 5N) onto the back of the peeled membrane. Ag paint was then used to mount the membranes onto a Ti foil, and electrodes were fabricated in the same way as for substrate-attached Si MW arrays.

C. Electrochemical characterization

The photoelectrochemical performance of each type of electrode was evaluated in an aqueous solution of potassium hydrogen phthalate (KHP, Sigma-Aldrich) that was buffered to pH = 4.5 using KOH.[7] Experiments were performed in a Pyrex electrochemical cell that had a flat side-facing window. A saturated calomel electrode (SCE) was used as the reference electrode, and either a carbon cloth or a Pt mesh electrode, separated from the working electrode compartment by a glass frit, was used as the counter electrode. During an experiment, both compartments of the cell were continuously purged with H_2 (Alphagaz1, Air Liquide).

Illumination was provided by either a 300 W tungsten–halogen ELH lamp (OSRAM) or by a Newport Oriel Xe lamp that was equipped with an AM 1.5G filter. The illumination intensity was varied by use of neutral density filters (Newport). The spectral irradiance of these light sources has been described previously.[6] The light intensity was calibrated using a Si photodiode (Thorlabs UDT UV-005) that had been mounted in the same orientation as the Si working electrodes. The electrolyte was stirred continuously with a magnetic stir bar to minimize mass-transport limitations and formation of bubbles on the electrode surface.

Before each set of experiments, all glassware in contact with the electrolyte was cleaned by soaking overnight in room-temperature *aqua regia* (3 : 1 $HCl : HNO_3$) and thoroughly rinsing with 18 MΩ cm resistivity water. After each set of experiments, a polished Pt disk was used to verify that the thermodynamic potential of the proton–hydrogen (H^+/H_2) redox couple was in agreement with that calculated by the Nernst equation. All potentials are reported relative to the reversible hydrogen electrode (RHE), which has a value of −0.51 V *vs.* SCE for an aqueous solution at pH 4.5. Before and after each set of experiments, a fresh planar p-Si electrode (ρ = 0.1 Ω cm) was cycled electrochemically 20–100 times at 100 mV s^{-1} between 0 and −0.6 V *vs.* RHE, to verify that no electrochemically active contaminants in the electrolyte were electrodeposited onto the working electrode under reducing conditions.

D. Catalyst deposition

Prior to electrodeposition of a catalyst, electrodes were treated in an O_2 plasma asher (March PX-500) at 300 W for 3 min under 300 mTorr of O_2, or were treated for 5–10 min in an UV/ozone cleaning system (BioForce UV/Ozone Procleaner Plus). Both processes removed residual PDMS from the Si surface and reacted with the PDMS infill to allow the aqueous electrolyte to penetrate between the wires. To remove any native surface oxides, the electrodes were then etched for 10 s in 10% HF (aq.).

Ni–Mo was electrodeposited from a bath that contained 1.3 M Ni^{II} sulfamate, 0.5 M H_3BO_3, and 20 mM Na_2MoO_4, with the pH adjusted to be ∼4.5 using KOH.[7] Electrodeposition was performed using a Princeton Applied Research Model 273 potentiostat, in a one-compartment cell, using a large area Ni mesh counter-electrode and a Ag/AgCl (3 M NaCl, E^o = +0.209 V *vs.* NHE) reference electrode. Samples were immersed in the deposition solution and illuminated at high intensity (∼400 mW cm^{-2}) with an ELH-type tungsten–halogen lamp. For galvanostatic depositions, the cathodic current densities were maintained at 20 mA cm^{-2} until a given total charge had passed (0.2–0.5 C cm^{-2}). For potentiostatic depositions, samples were held at −1 V *vs.* the reference electrode until 0.2–0.5 C cm^{-2} of charge density had passed. The structure and morphology of the electrodeposited catalyst were characterized using a field-emission scanning electron microscope (Zeiss 1550VP). The Ni–Mo electrodeposition process did not allow for significant tuning of the composition of the Ni–Mo. Little or no active catalyst deposition was observed when the deposition potential was varied or when the ratio of Ni^{II} sulfamate to Na_2MoO_4 was changed in the plating bath.

Control devices that used Pt as an HER catalyst were produced by using electron-beam evaporation to deposit 1.5–2 nm planar equivalents of high-purity Pt (Kurt Lesker, 4N) at a rate of 0.01–0.05 nm s^{-1} onto the Si wire arrays. Immediately before deposition, the Si MW array samples were briefly etched in buffered HF, to remove native oxides.

E. Spectral response

Photoelectrochemical spectral response measurements were performed using illumination from a 150 W Xe lamp that was passed through an Oriel monochromator (0.5 mm slits), then chopped at ∼30 Hz, and focused to a beam spot that under-filled the electrode area (∼0.05 cm^2) in solution. A calibrated Si diode (Thorlabs UDT UV-050) was used to measure the light intensity incident on the electrode. Another Si photodiode was used to measure a beam-split portion of the illumination, with this Si photodiode providing a continuous calibration of the light intensity output from the monochromator. A potentiostat (Gamry Series G 300) was used to maintain the potential of the Si working electrode at the formal potential for H_2-evolution (E = 0 *vs.* RHE) and to record the current produced by the sample. The chopped components of the signals were measured by use of independent lock-in detection of the sample channel (the analog output of the potentiostat) and the calibration channel (the beam-split illumination on the photodiode), respectively.[6]

F. Calculation of photocathode efficiency

The performance of each electrode was evaluated using standard performance metrics for photovoltaic devices, with potentials calculated relative to the reversible hydrogen electrode (E_{RHE}).[7]

$$V_{oc} = E_{oc} - E_{RHE} \quad (1)$$

$$J_{sc} = |J|_{E_{RHE}} \quad (2)$$

$$ff = \frac{P_{max}}{V_{oc} \cdot J_{sc}} \quad (3)$$

$$\eta_{H_2} = \frac{ff \cdot V_{oc} \cdot J_{sc}}{P_{in}} = \frac{-i_{max}(E_{max} - E_{RHE})}{P_{in} \cdot A} \quad (4)$$

The open-circuit voltage (V_{oc}) of a photoelectrode is a measure of the maximum free energy generated by the system relative to the thermodynamic HER potential under the specified experimental conditions. The value of V_{oc} was calculated as the difference between the potential at which the photoelectrode passed no current (E_{oc}) and the real hydrogen electrode potential (E_{RHE}) measured during the experiments (eqn (1)). This V_{oc} is the photovoltage that would be produced in a regenerative two-electrode cell in which the counter electrode was performing the oxidation of H_2 to H^+. Accordingly, the short-circuit current density (J_{sc}) was determined by measurement of the current density at E_{RHE} (eqn (2)). The fill factor (*ff*) of the device quantifies how the maximum power density (P_{max}) attained by the photoelectrode at potentials positive of E_{RHE} compares to the product of V_{oc} and J_{sc} (eqn (3)). The photocathode efficiency was calculated as the ratio of P_{max} to the incoming light intensity. The efficiency can be equivalently defined in terms of the *ff*, V_{oc}, and J_{sc} or in terms of the current and voltage measured at the maximum power point (i_{max} and E_{max}) (eqn (4)). The errors reported in all measured values represent a 1σ confidence interval.

Efficiencies that are calculated in this fashion do not include resistance losses that would be present in a two-electrode cell, nor do these efficiencies account for polarization losses at the counter electrode. The values are thus reported as single photoelectrode efficiencies for the working electrode, as opposed to efficiencies for the overall water-splitting reaction. In this work, the calculated photoelectrode efficiencies are referenced directly to the behavior of an ideally nonpolarizable working electrode, and thus all photoelectrode potentials are referenced to the thermodynamically reversible potential, E_{RHE}. The use of a thermodynamically measured reference allows facile and consistent comparison between the behavior of semiconductor–catalyst composites with varying compositions and in various electrolytes, provided that E_{RHE} is well defined for the electrolyte system of interest. Coupling the single-electrode measurements used herein with analogous measurements for photoanodes also allows prediction of the operating current density, and overall efficiency, of a tandem water-splitting cell.[18]

The maximum power point for fuel-forming photocathodes has alternatively been calculated by comparing the behavior of the photo-responsive working electrode to the *J*–*E* behavior of a clean Pt working electrode measured under nominally the same conditions as the photoelectrode.[14,15] These "power saved" efficiencies are therefore subject to the properties of the working electrode and electrochemical cell that has been selected to be the "reference system." Efficiency values that are calculated in this alternative fashion are higher than the ones quoted herein because the "power saved" efficiencies account for kinetic and concentration overpotential losses at the selected Pt working electrode as well as for uncompensated resistance losses in the electrolyte.

Results

Fig. 1 displays the fabrication process that was used to prepare the Si MW array photocathodes, along with SEM images of representative Si MW arrays at the initial and final stages of device processing. The as-grown wires were 1.8–2.3 μm in diameter and ranged in height from 60–100 μm (Fig. 1A). Before formation of an n^+p junction onto these Si MWs, the Cu VLS catalyst was removed, and a thermal oxide was grown over the wires (Fig. 1B). The bottom 10–20 μm of each wire was then protected with PDMS, and the oxide was etched off the tops of the wires (Fig. 1C). After doping to form an n^+-Si emitter (Fig. 1D), the wire arrays were filled with PDMS and scattering particles (Fig. 1E). Samples were then fabricated into electrodes, either on the substrate or peeled from the substrate (not shown), before the catalyst material was deposited (Fig. 1F) and the resulting device performance was evaluated. Fig. 1G displays an SEM image of the as-grown wires, and Fig. 1H displays an SEM image of the n^+p-Si MW with the deposited Ni–Mo catalyst.

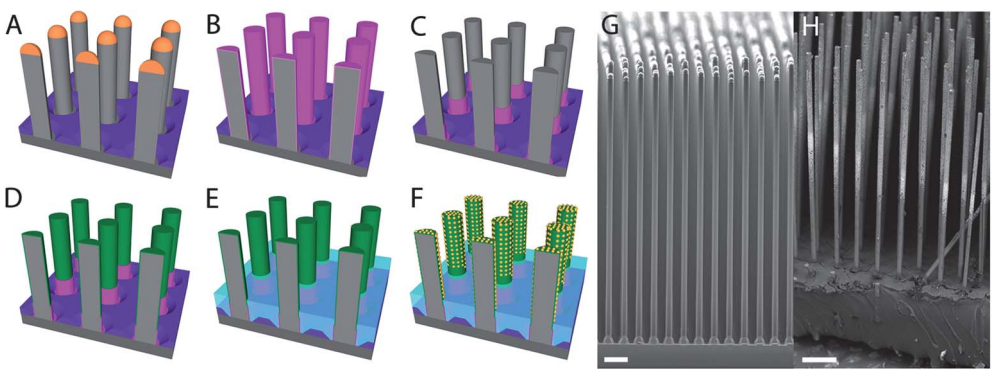

Fig. 1 Schematic of Device Fabrication. Ni–Mo-coated n^+p-Si MW photocathode devices were fabricated using the steps outlined above. (A) As-grown VLS Si MW wire array. (B) VLS wires after catalyst removal and thermal oxide growth. (C) p-Si MW array with oxide boots. (D) n^+p-Si MW array after diffusion. (E) n^+p-Si MW array infilled with scattering particles and PDMS. (F) n^+p-Si MW devices with electrodeposited Ni–Mo catalyst. (Peeled devices were removed from the substrate before catalyst deposition.) (G) SEM image of as-grown wires (schematic A). (H) SEM image of a fully processed device (schematic F). All scale bars are 10 μm.

A. Characterization of the Si n^+p junction

The doping densities and electrical properties of the n^+p-Si MW devices were characterized by solid-state measurements. Four-point probe measurements indicated that the electronically active dopant densities of the as-grown p-Si wires were $N_A = \sim 1.5 \times 10^{17}$ cm^{-3}.[16] Two-point measurements made on single n^+p junction wires by separately contacting the n^+-Si emitter and the p-Si base produced open-circuit voltages (V_{oc}) of 489 ± 12 mV and fill factors (*ff*) of 0.73 ± 0.04 under simulated AM 1.5G solar illumination.

B. Catalyst deposition

Ni–Mo was deposited using both galvanostatic and potentiostatic deposition methods. When galvanostatic deposition was used on n^+p junction wires, most of the catalyst material deposited at the base of the wire array (Fig. 2A). This morphology resulted in catalytic performance with low fill factors during the electrochemical characterization of the devices (see ESI†). If the polymer infill did not cover the interface between the p-Si and n^+-Si emitter, Ni–Mo preferentially deposited at this junction, and shunting of the device was observed (Fig. 2B).

Potentiostatic deposition from the Ni–Mo bath produced a uniform morphology of 100–200 nm diameter clumps, with a heavier catalyst loading at the tops of the wires (Fig. 2C and D). Optimal catalyst loading was achieved by passage of 0.2 to 0.5 C cm^{-2} of cathodic charge density during catalyst deposition. When the nominally identical potentiostatic deposition protocol for Ni–Mo was performed on planar n^+p junction Si photocathodes, the current density of the deposition exceeded 100 mA cm^{-2}, and the catalyst material readily delaminated from the surface, resulting in unstable HER activity. In contrast, when the catalyst was deposited by pulsed potentiostatic depositions (cycled between applying −1 V *vs.* Ag/AgCl for 0.05 C cm^{-2} and holding the electrode at open circuit for 3 s) or was deposited by galvanostatic deposition at −20 mA cm^{-2}, Ni–Mo adhered well to planar electrodes. Energy dispersive spectroscopy measurements indicated that the deposited Ni–Mo alloys were ~85% Ni and ~15% Mo, similar to the composition obtained previously for electrodeposited films.[7]

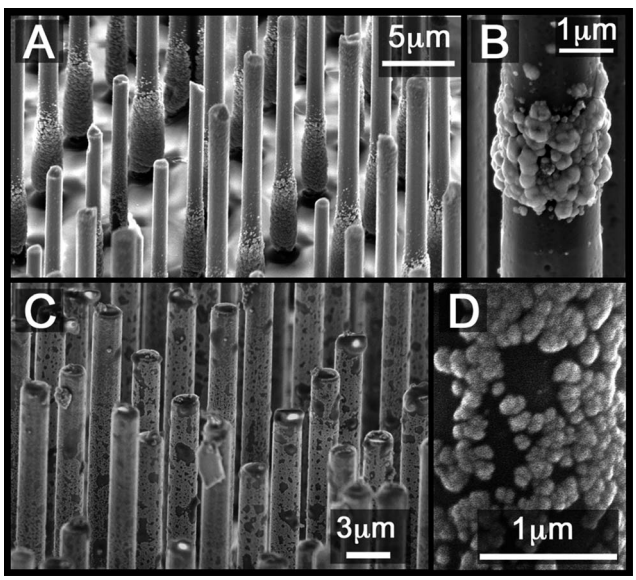

Fig. 2 SEM images of Ni–Mo particles on n^+p-Si MWs under different deposition conditions. (A) Galvanostatic deposition (all catalyst at bottom), (B) deposition with no infill (Ni–Mo deposits at junction), (C) potentiostatic deposition (uniform catalyst coverage), (D) high magnification image of Ni–Mo from potentiostatic deposition.

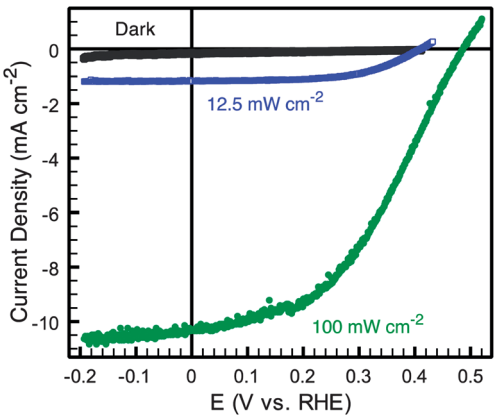

Fig. 3 *J–E* data for a representative Ni–Mo-coated n^+p-Si MW array photocathode measured in H_2-purged pH 4.5 KHP buffer under ELH-type illumination. *J–E* data were collected by sweeping the potential from negative to positive at 30 mV s^{-1}, and are referenced to the reversible hydrogen potential in the solution ($E(H^+/H_2) = -0.51$ V *vs.* SCE).

C. Current density *vs.* potential behavior

The current density *vs.* potential behavior of representative Si MW array samples, in contact with pH = 4.5 aqueous KHP solutions, was examined before and after catalyst deposition. Under 100 mW cm^{-2} of ELH-type illumination, planar n^+p-Si photocathodes without any deliberate catalyst deposition exhibited light-limited photocurrent densities (J_{ph}) of 29.6 ± 1.5 mA cm^{-2} (at −0.8 V *vs.* RHE), whereas n^+p-Si MW photocathodes exhibited $J_{ph} = 16.4 \pm 1.8$ mA cm^{-2} (at −0.6 *vs.* RHE). Fig. 3 displays representative *J–E* data for 80–90 μm long n^+p-Si MW arrays that had been coated with Ni–Mo, while Table 1

Table 1 Figures of merit for representative HER photocathodes, measured in H_2-purged pH 4.5 KHP buffer under 100 mW cm^{-2} ELH-type solar illumination. For all Ni–Mo data, the catalyst was electrodeposited onto the Si device. For all devices with Pt, 1.5–2.0 nm of Pt catalyst was evaporated using an e-beam evaporator immediately before electrochemical testing. The devices with Pt were tested after all the Ni–Mo devices, to minimize any Pt contamination of the electrolyte

Sample type	V_{oc} (mV)	J_{sc} (mA cm^{-2})	*ff*	η (%)	#
Ni-Mo/n^+p-Si MW (with scatterers)	457 ± 34	9.1 ± 2.11	0.46 ± .03	1.9 ± 0.4	5
Best device	485	10.3	0.45	2.2	1
Ni–Mo/n^+p-Si MW (no scatterers)	496 ± 5	5.5 ± 0.6	0.42 ± .08	1.1 ± 0.2	6
Ni–Mo/p-Si MW	139 ± 31	6.7 ± 0.6	0.24 ± .03	0.22 ± 0.1	3
Ni–Mo/n^+p planar	526 ± 23	22.3 ± 2.6	0.31 ± .03	3.6 ± .01	5
Pt/n^+p-Si MW (no scatterers)	441 ± 14	13.2 ± 5.8	0.47 ± .08	2.7 ± 1.3	5
Pt/n^+p planar	537 ± 19	32.3 ± 4.0	0.44 ± .07	7.54 ± 0.4	3

contains the data for all the types of electrodes tested. Under 100 mW cm^{-2} of ELH illumination, the champion device exhibited $V_{oc} = 0.485$ V, $J_{sc} = 10.3$ mA cm^{-2}, $ff = 0.45$, and a photoelectrode energy-conversion efficiency for H_2 evolution (η_{H_2}) of 2.2%. Under these conditions, the average performance of Ni–Mo-coated n^+p-Si MW electrodes ($V_{oc} = 0.46$ V, $J_{sc} = 9.1$ mA cm^{-2}, $ff = 0.46$, $\eta = 1.9\%$) was comparable to Si MW array electrodes that had Pt as the HER catalyst ($V_{oc} = 0.44$ V, $J_{sc} = 13.2$ mA cm^{-2}, $ff = 0.47$, $\eta = 2.7\%$). In contrast, Ni–Mo coated p-Si MW arrays that did not have n^+ emitter layers or scatters exhibited $V_{oc} = 0.14$ V, $J_{sc} = 6.7$ mA cm^{-2}, $ff = 0.24$ and $\eta_{H_2} = 0.22\%$ (Table 1). After the arrays were scraped from the degenerately doped Si(111) growth substrates, the substrates themselves exhibited negligible photoactivity for H_2 evolution.

D. Freestanding polymer-supported photoactive membranes

When flexible, polymer-supported Ni–Mo-coated n^+p-Si MW array structures were removed from the Si substrate and used as photocathodes, the measured V_{oc} (475 ± 11 mV) was very similar to that displayed by the substrate-attached Si MW arrays. However, the polymer-supported devices exhibited low photocurrent densities (0.44 ± 0.05 mA cm^{-2}), due to non-uniform back contacts to the flexible Si MW-embedded membranes (Fig. 4).

E. Stability

Fig. 5 shows the performance of a representative Ni–Mo-coated n^+p-Si MW photoelectrode that was held at $E = 0.0$ V *vs.* RHE for >60 min under 100 mW cm^{-2} of ELH illumination, with a full set of *J*–*E* data collected at 10 min intervals. Over this time period, the V_{oc} remained nearly constant, but J_{sc} decreased from 10.1 to 9.2 mA cm^{-2}. The inset shows the current density *vs.* time for steady-state operation, during which the potential of the electrode was maintained $E = 0.0$ V *vs.* RHE.

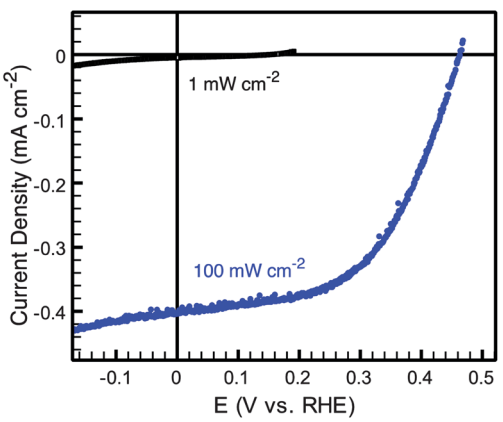

Fig. 4 *J*–*E* data for a Ni–Mo/n^+p-Si MW photocathode device peeled from the substrate. Electrical contact was made to the back of the sample by evaporating Au, and then pasting the Si MW/PDMS film onto Ti foil using conductive Ag paint. Data were collected in H_2-purged pH 4.5 KHP buffer under ELH-type illumination. The *J*–*E* data were collected by sweeping the potential from negative to positive at 30 mV s^{-1} and are referenced to the reversible hydrogen potential in the solution ($E(H^+/H_2) = -0.51$ V *vs.* SCE).

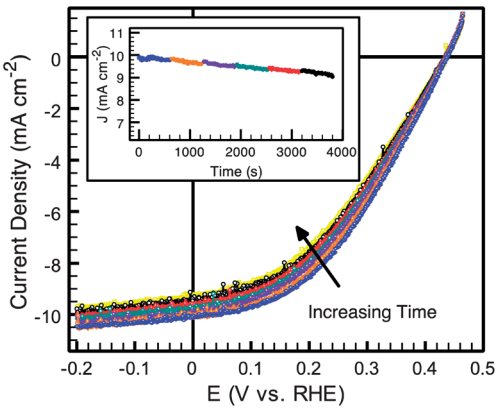

Fig. 5 Stability testing of a representative Ni–Mo-coated n^+p-Si MW photoelectrode in H_2-purged pH 4.5 KHP buffer. *J*–*E* data were taken every 10 min under 100 mW cm^{-2} of ELH-type illumination. The electrode was held at short circuit, *i.e.* at 0 V *vs.* RHE, between the collection of each dataset (shown in inset).

F. Spectral response

Fig. 6A shows the external quantum yield (EQY) of Ni–Mo coated n^+p junction Si MW array and planar n^+p-Si electrodes as a function of wavelength. The external quantum yield of vertically oriented Si MW arrays depends on the angle of illumination, so the electrodes were tilted slightly to maximize their current densities.[6,17] After recording the spectral response data, the performance of the photocathodes was measured with cyclic voltammetry under 100 mW cm^{-2} of ELH-type illumination (Fig. 6B). For comparison, data are also depicted for a planar n^+p junction that had low (0.15 C cm^{-2}) and high (0.3 C cm^{-2}) catalyst loadings, respectively. At low loadings of Ni–Mo, the planar sample exhibited $J_{sc} = 21.8$ mA cm^{-2}, $V_{oc} = 560$ mV, $ff = 0.28$, and $\eta_{H_2} = 3.5\%$. At higher catalyst loading, such electrodes exhibited $J_{sc} = 8.6$ mA cm^{-2}, $V_{oc} = 469$ mV, $ff = 0.45$ and $\eta_{H_2} = 1.8\%$. After measurement of the spectral response, the Ni–Mo-coated n^+p-Si MW device exhibited $J_{sc} = 9.4$ mA cm^{-2}, $V_{oc} = 447$ mV, $ff = 0.51$, and $\eta_{H_2} = 2.1\%$.

Discussion

A. Catalyst morphology

The composition and particle morphology of the Ni–Mo catalyst films that were prepared in this work are very similar to those obtained previously by the use of galvanostatic deposition.[7] Under galvanostatic conditions, the catalyst material was observed to deposit predominantly at the base of the wires, for both p-Si MW array and n^+p-Si MW array devices. Generation of 20 mA cm^{-2} of current density from the Si MW array electrodes during electrodeposition of the catalyst resulted in a working electrode potential of −0.7 V *vs.* Ag/AgCl. Under potentiostatic conditions at more negative electrode potentials (−1 V *vs.* Ag/AgCl), the deposition proceeded at higher current densities (80–100 mA cm^{-2}) and required a much shorter period of time (1–3 s) to pass the specified amount of cathodic charge density. At these high current densities, the Ni–Mo deposition proceeded more uniformly across the surface of the microwires, possibly due to tuning of the interplay between hydrogen evolution and metal deposition (Fig. 2C).

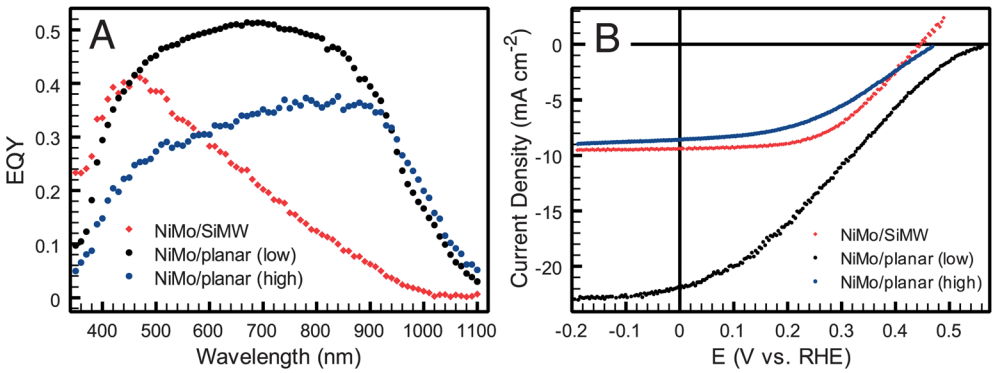

Fig. 6 (A) Spectral response (external quantum yield (EQY) *vs.* wavelength) data collected for Ni–Mo-coated n^+p-Si MW photocathodes (red diamonds), and planar Ni–Mo-coated n^+p-Si photocathodes under high (blue circles) and low (black circles) catalyst loading. (B) Corresponding *J*–*E* data for the same electrodes under 100 mW cm^{-2} of ELH-type illumination. All the data were collected in H_2-purged pH 4.5 KHP buffer.

When Ni–Mo was coated onto Si MW array electrodes, a tradeoff was observed between obtaining optimal electrocatalytic properties for H_2 evolution and minimizing undesirable optical absorption and reflection due to the presence of the catalyst particles. Even with the addition of scattering particles, the highest observed J_{sc} value observed for Ni–Mo coated Si MW array electrodes was ~10 mA cm^{-2}, whereas under the same illumination conditions, Pt-coated Si MW array electrodes without scatterers exhibited $J_{sc} = 13.2$ mA cm^{-2}. Ni–Mo-coated Si MW array devices that did not contain scattering particles at the bases of the Si MWs exhibited $J_{sc} \sim 5$ mA cm^{-2} (Table 1). Optimally performing devices had catalyst loadings that decreased J_{sc} by only 25–35% relative to the light-limited current density that was measured before catalyst deposition. Increased catalyst loadings improved the fill factors of the *J*–*E* data, but resulted in significant decreases in photocurrent density and energy-conversion efficiency of the photoelectrodes.

B. Current density *vs.* potential behavior

The introduction of an emitter, to produce radial n^+p junctions on the p-Si MWs, increased all of the figures of merit for photoelectrochemical hydrogen production, relative to p-type Si MW arrays that did not contain the emitter layer (Table 1). This decoupling of the voltage-producing junction from the catalytic reaction thus provides more control over the design of the MW array electrodes for solar-fuel generation. Formation of a Si n^+p homojunction produces a photovoltage that is not dependent on the pH of the electrolyte.[18] The V_{oc} measured for the Si MW array photoelectrode was within 40 mV of V_{oc} measured for the Si MW array solid-state device. The high photovoltages observed for the freestanding, polymer-supported membrane-based devices, and the lack of observable photocurrent from the degenerately doped planar Si substrates, demonstrate that the photovoltage was predominantly produced by the n^+p-Si MW array portion of the device.

Many prior reports of Si-based photocathodes for the HER have used noble metals as the HER catalyst, and data were reported under strongly acidic conditions. In general, non-noble metal electrocatalysts for the HER exhibit limited stability under acidic conditions. The pH = 4.5 electrolyte was chosen so that the resulting photocathode performance data could be directly compared to prior electrochemical studies of the same catalyst for the HER.[7] Polarization data measured with a Pt disk yielded a much less pronounced increase in cathodic HER current density as the electrode potential was made more negative in pH 4.5 KHP buffer than in 0.5 M H_2SO_4 (see ESI†).[19] At this mildly acidic pH, the reaction mechanism is potentially complex, because both H_2O and H_3O^+ can serve as the proton source for the generation of H_2.[20] This change in electrolyte pH accounts for the change in fill factor between the data presented herein relative to prior reports of similar structures, which have displayed fill factors of 0.7, in 0.5 M H_2SO_4.[6] Identification of the conditions that optimally balance the stability of the catalyst/semiconductor system, while maximizing the behavior of the catalytic onset, is of continued interest.

Ni–Mo has been shown to be extremely stable under alkaline conditions.[21,22] The stability data shown (Fig. 5) demonstrate that the Ni–Mo/Si system is a promising candidate to serve as an HER photocathode at other pH values as well. The observed decrease in J_{sc} and *ff* over time can be at least partially attributed to delamination of the catalyst due to H_2 bubble formation.[21] A second electrodeposition of catalyst onto the electrode after initial testing consistently restored the catalytic turn-on behavior to its initial state.

C. Balancing catalytic activity and short-circuit current density

Fig. 7A shows the calculated *ff* *vs.* the measured J_{sc} values for several representative planar and Si MW array devices. The decrease in *ff* at higher J_{sc} values (corresponding to higher illumination intensity) reveals an important design constraint for integrated solar-fuel generating systems. The turnover limitations of the catalyst and the limitations of majority-carrier flow within the semiconductor lead to series-resistance losses in the performance of the both planar and microwire array devices.[23] However, under equivalent illumination conditions, the fill factors for the Si MW samples were significantly greater than those of the planar control samples. This observation is consistent with expectations that the enhanced surface area of the wire arrays provides an advantage in the effective catalytic turn-on of these devices. Fig. 7B shows the voltage loss (V_{loss}, calculated as the difference between E_{oc} and the potential of the maximum power point, E_{max}) of the photoelectrodes. The *ff* and V_{loss} data

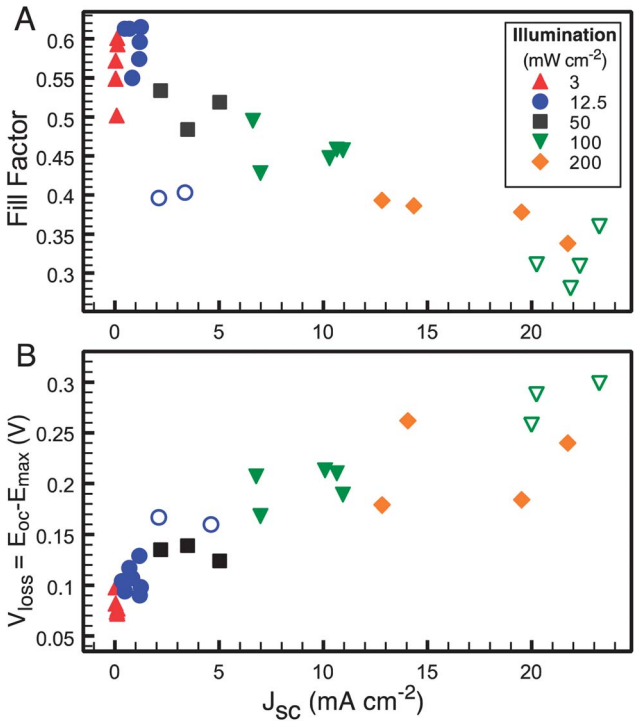

Fig. 7 (A) Comparison of fill factor *vs.* the attainable J_{sc} at a variety of light intensities for Ni–Mo-coated radial n^+p junction Si MW (closed symbols) and planar n^+p-Si (open symbols) electrodes in H_2-purged pH 4.5 KHP buffer over a range of light intensities. (B) The voltage loss (calculated as the difference between the open-circuit potential and the potential of the maximum power point, E_{max}) for the same samples and conditions.

follow the same trend, indicating that the onset of catalytic behavior near open-circuit conditions, and not just J_{sc}, has an impact on the performance of the devices. The MW geometry minimizes overpotential losses, which is important for photoelectrochemical fuel-forming reactions that will not proceed unless sufficient potential is generated to drive both of the electrochemical reactions in a full fuel-forming process.

D. Spectral response

At low loading of Ni–Mo, the planar electrode showed an EQY = ~0.5, which is 25% lower then the EQY reported previously for similar devices that had been coated with a thin Pt catalyst.[6] Still further increases in the catalyst loading decreased the EQY to ~0.3%. However, the spectral response data, which were collected under short-circuit conditions, do not provide information about how the system operates under maximum power conditions. A comparison of the *J–E* performance at high and low catalyst loadings reveals that although the J_{sc} was much higher in the case of low catalyst loading, the catalytic behavior was limiting, and resulted in a poor *ff* and thus produced only a slight increase in conversion efficiency at the maximum power point. Wire arrays that had an optimal catalyst loading outperformed the planar devices with high catalyst loading in *ff* as well with respect to their overall photoelectrode solar energy-conversion efficiencies. The spectral response data for the wire arrays (Fig. 6A) were similar to behavior reported previously, but were uniformly lower in magnitude due to the higher loading levels of the Ni–Mo catalyst relative to a thin Pt film.[6] When illuminated with blue wavelengths, the wire arrays performed similarly to planar devices, whereas non-optimized light trapping, and concomitant absorption of photons in the degenerately doped substrate limited the red-wavelength response of such systems.

E. Freestanding polymer-supported photoactive membranes

A membrane-based artificial photosynthesis assembly would allow the photoanode and photocathode materials to be in electrical contact, while separating the gaseous products and allowing ions to pass in order to maintain charge neutrality.[24] Si MW arrays have been embedded in a membrane consisting of Nafion® (a perfluorosulfonic acid polytetrafluoroethylene copolymer) and poly(3,4-ethylenedioxythiophene)–poly(styrene sulfonate) (PEDOT–PSS), and have been shown to be mechanically stable and exhibit limited H_2 crossover.[25] Si MW arrays have also previously been removed from the growth substrate and evaluated as photocathodes in a flexible, freestanding membrane that contained a polymer support and embedded Si MWs.[2] In this work, we demonstrated that catalyst-coated, n^+p-Si MW arrays can be peeled from the substrate while maintaining the high photovoltage that is generated in each individual Si MW. When embedded in PDMS and removed from the growth substrate, the n^+p-Si MW array membranes coated with Ni–Mo produced $V_{oc} = 475$ mV, which is greater than the V_{oc} observed for the unpeeled devices. The measured photocurrents for these devices were significantly lower than for the substrate-attached Si MW arrays, but the non-uniformity of the catalyst deposition suggests that not all the wires were successfully back-contacted. Improvement in the electrical contacting scheme for a flexible membrane therefore remains of interest in the development of a complete artificial photosynthetic device.[26,27]

Conclusions

Arrays of radial junction n^+p-Si MWs have been coupled to earth-abundant Ni–Mo catalysts and investigated as photocathodes for the hydrogen evolution reaction. These devices show that Ni–Mo alloys can be directly coupled to high-performance semiconductor absorbers to drive the HER at efficiencies comparable to rarer catalysts such as Pt, with promising stability under mildly acidic conditions. The balance between catalytic activity and photocurrent is an important design parameter for direct solar-fuel conversion devices. The ability to remove the wire arrays from the substrate, while maintaining high open-circuit voltages, is an important step in the development of a scalable, membrane-based, solar water-splitting prototype.

Acknowledgements

ELW and NSL acknowledge support from the Department of Energy (DE-FG02-05ER15754) for Si MW growth and device fabrication. JRM and HBG acknowledge support from the National Science Foundation (NSF) Powering the Planet Center for Chemical Innovation (CHE-0802907) for catalyst preparation and characterization. The authors would like to thank Hal Emmer, Dan Turner-Evans, and Elizabeth Santori for help with

device fabrication and spectral response data collection. We acknowledge critical support and infrastructure provided for this work by the Kavli Nanoscience Institute at Caltech. JRM would like to thank the Department of Energy, Office of Science, for a graduate research fellowship.

References

1 B. M. Kayes, H. A. Atwater and N. S. Lewis, *J. Appl. Phys.*, 2005, **97**, 114302.
2 J. M. Spurgeon, S. W. Boettcher, M. D. Kelzenberg, B. S. Brunschwig, H. A. Atwater and N. S. Lewis, *Adv. Mater.*, 2010, **22**, 3277–3281.
3 S. W. Boettcher, J. M. Spurgeon, M. C. Putnam, E. L. Warren, D. B. Turner-Evans, M. D. Kelzenberg, J. R. Maiolo, H. A. Atwater and N. S. Lewis, *Science*, 2010, **327**, 185–187.
4 M. D. Kelzenberg, D. B. Turner-Evans, M. C. Putnam, S. W. Boettcher, R. M. Briggs, J. Y. Baek, N. S. Lewis and H. A. Atwater, *Energy Environ. Sci.*, 2011, **4**, 866–871.
5 M. C. Putnam, S. W. Boettcher, M. D. Kelzenberg, D. B. Turner-Evans, J. M. Spurgeon, E. L. Warren, R. M. Briggs, N. S. Lewis and H. A. Atwater, *Energy Environ. Sci.*, 2010, **3**, 1037–1041.
6 S. W. Boettcher, E. L. Warren, M. C. Putnam, E. A. Santori, D. Turner-Evans, M. D. Kelzenberg, M. G. Walter, J. R. McKone, B. S. Brunschwig, H. A. Atwater and N. S. Lewis, *J. Am. Chem. Soc.*, 2011, **133**, 1216–1219.
7 J. R. McKone, E. L. Warren, M. J. Bierman, S. W. Boettcher, B. S. Brunschwig, N. S. Lewis and H. B. Gray, *Energy Environ. Sci.*, 2011, **4**, 3573–3583.
8 Y. Hou, B. L. Abrams, P. C. K. Vesborg, M. E. Björketun, K. Herbst, L. Bech, A. M. Setti, C. D. Damsgaard, T. Pedersen, O. Hansen, J. Rossmeisl, S. Dahl, J. K. Nørskov and I. Chorkendorff, *Nat. Mater.*, 2011, **10**, 434–438.
9 R. E. Rocheleau, E. L. Miller and A. Misra, *Energy Fuels*, 1998, **12**, 3–10.
10 S. Y. Reece, J. A. Hamel, K. Sung, T. D. Jarvi, A. J. Esswein, J. J. H. Pijpers and D. G. Nocera, *Science*, 2011, **334**, 645–648.
11 Z. Chen, D. Cummins, B. N. Reinecke, E. Clark, M. K. Sunkara and T. F. Jaramillo, *Nano Lett.*, 2011, **11**, 4168–4175.
12 K. Sun, K. Madsen, P. Andersen, W. N. Bao, Z. L. Sun and D. L. Wang, *Nanotechnology*, 2012, **23**, 194013.
13 S. Takayama, E. Ostuni, X. Qian, J. C. McDonald, X. Jiang, P. LeDuc, M. H. Wu, D. E. Ingber and G. M. Whitesides, *Adv. Mater.*, 2001, **13**, 570–574.
14 A. Heller and R. G. Vadimsky, *Phys. Rev. Lett.*, 1981, **46**, 1153–1156.
15 E. Aharon-Shalom and A. Heller, *J. Electrochem. Soc.*, 1982, **129**, 2865–2866.
16 M. D. Kelzenberg, D. B. Turner-Evans, B. M. Kayes, M. A. Filler, M. C. Putnam, N. S. Lewis and H. A. Atwater, *Nano Lett.*, 2008, **8**, 710–714.
17 M. D. Kelzenberg, S. W. Boettcher, J. A. Petykiewicz, D. B. Turner-Evans, M. C. Putnam, E. L. Warren, J. M. Spurgeon, R. M. Briggs, N. S. Lewis and H. A. Atwater, *Nat. Mater.*, 2010, **9**, 239–244.
18 E. L. Warren, S. W. Boettcher, M. G. Walter, H. A. Atwater and N. S. Lewis, *J. Phys. Chem. C*, 2010, **115**, 594–598.
19 S. Schuldiner, *J. Electrochem. Soc.*, 1954, **101**, 426–432.
20 M. G. Walter, E. L. Warren, J. R. McKone, S. W. Boettcher, Q. Mi, E. A. Santori and N. S. Lewis, *Chem. Rev.*, 2010, **110**, 6446–6473.
21 D. E. Brown, M. N. Mahmood, M. C. M. Man and A. K. Turner, *Electrochim. Acta*, 1984, **29**, 1551–1556.
22 D. E. Brown, M. N. Mahmood, A. K. Turner, S. M. Hall and P. O. Fogarty, *Int. J. Hydrogen Energy*, 1982, **7**, 405–410.
23 J. Nelson, *The Physics of Solar Cells*, Imperial College Press, London, 2003.
24 N. S. Lewis and D. G. Nocera, *Proc. Natl. Acad. Sci. U. S. A.*, 2007, **104**, 20142.
25 J. M. Spurgeon, M. G. Walter, J. Zhou, P. A. Kohl and N. S. Lewis, *Energy Environ. Sci.*, 2011, **4**, 1772–1780.
26 S. L. McFarlane, B. A. Day, K. McEleney, M. S. Freund and N. S. Lewis, *Energy Environ. Sci.*, 2011, **4**, 1700–1703.
27 I. Yahyaie, K. McEleney, M. Walter, D. R. Oliver, D. J. Thomson, M. S. Freund and N. S. Lewis, *J. Phys. Chem. Lett.*, 2011, **2**, 675–680.